





Vesicular Acetylcholine Transporter Alters Cholinergic Tone and Synaptic Plasticity in DYT1 Dystonia

Annalisa Tassone, PhD,¹  Giuseppina Martella, PhD,¹  Maria Meringolo, PhD,¹ Valentina Vanni, PhD,¹ Giuseppe Sciamanna, PhD,¹ Giulia Ponterio, PhD,¹ Paola Imbriani, MD,¹ Paola Bonsi, PhD,¹  and Antonio Pisani, MD, PhD^{2,3*} 

¹Laboratory of Neurophysiology and Plasticity, IRCCS Fondazione Santa Lucia, Rome, Italy

²Department of Brain and Behavioral Sciences, University of Pavia, Pavia, Italy

³IRCCS Mondino Foundation, Pavia, Italy

ABSTRACT: Background: Acetylcholine-mediated transmission plays a central role in the impairment of corticostriatal synaptic activity and plasticity in multiple DYT1 mouse models. However, the nature of such alteration remains unclear.

Objective: The aim of the present work was to characterize the mechanistic basis of cholinergic dysfunction in DYT1 dystonia to identify potential targets for pharmacological intervention.

Methods: We utilized electrophysiology recordings, immunohistochemistry, enzymatic activity assays, and Western blotting techniques to analyze in detail the cholinergic machinery in the dorsal striatum of the Tor1a^{+/-} mouse model of DYT1 dystonia.

Results: We found a significant increase in the vesicular acetylcholine transporter (VACHT) protein level, the protein responsible for loading acetylcholine (ACh) from the cytosol into synaptic vesicles, which indicates an altered cholinergic tone. Accordingly, in Tor1a^{+/-} mice we measured a robust elevation in basal ACh content coupled to a compensatory enhancement of acetylcholinesterase (AChE) enzymatic activity.

Moreover, pharmacological activation of dopamine D2 receptors, which is expected to reduce ACh levels, caused an abnormal elevation in its content, as compared to controls. Patch-clamp recordings revealed a reduced effect of AChE inhibitors on cholinergic interneuron excitability, whereas muscarinic autoreceptor function was preserved. Finally, we tested the hypothesis that blockade of VACHT could restore corticostriatal long-term synaptic plasticity deficits. Vesamicol, a selective VACHT inhibitor, rescued a normal expression of synaptic plasticity.

Conclusions: Overall, our findings indicate that VACHT is a key player in the alterations of striatal plasticity and a novel target to normalize cholinergic dysfunction observed in DYT1 dystonia. © 2021 The Authors. *Movement Disorders* published by Wiley Periodicals LLC on behalf of International Parkinson and Movement Disorder Society

Key Words: acetylcholine; striatum; cholinergic interneurons; vesicular acetylcholine transporter; acetylcholinesterase

This is an open access article under the terms of the Creative Commons Attribution License, which permits use, distribution and reproduction in any medium, provided the original work is properly cited.

*Correspondence to: Dr. A. Pisani, Department of Brain and Behavioral Sciences, University of Pavia, Pavia, Italy, and IRCCS Mondino Foundation, Pavia, Italy; E-mail: antonio.pisani@unipv.it; antonio.pisani@mondino.it

Relevant conflicts of interests/financial disclosures: A.P. is employed at the University of Pavia, Pavia, Italy; P.B. and P.I. are employed at Fondazione Santa Lucia, Rome, Italy; A.P. holds grants that are not related to the subject of the present study. A.T., G.M., M.M., V.V., G.S., G.P., P.I., P.B., and A.P. declare the absence of any potential conflicts of interest. The authors report no biomedical financial interests or potential conflicts of interest.

Funding agencies: This project was supported by the 2019 Bachmann-Strauss Prize for Excellence in Dystonia Research to A.P. The Italian Ministry of Health supported this project, under the frame of EJP RD, the European Joint Programme on Rare Diseases (EJP RD-135 2019) to A.P. In addition, this project has received funding from the European Union's Horizon 2020 research and innovation program under the EJP RD COFUND-EJP no. 825575 (EurDyscover) to A.P.

Received: 30 November 2020; **Revised:** 18 May 2021; **Accepted:** 7 June 2021

Published online 26 June 2021 in Wiley Online Library (wileyonlinelibrary.com). DOI: 10.1002/mds.28698

Dystonia is a common movement disorder characterized by sustained, repetitive muscle contractions, twisting movements, and abnormal postures.¹ Deletion of three base pairs (Δ GAG) in the *TOR1A* gene results in the loss of a glutamic acid in the C-terminal of the protein torsinA that is associated to early-onset generalized dystonia (DYT1).² Currently, the precise function of torsinA remains unclear, although it plays a role in multiple cellular activities, including protein folding, protein quality control of the endoplasmic reticulum, control of secretion, lipid metabolism, trafficking, degradation, and nuclear envelope dynamics.³⁻⁷

Anticholinergic drugs are among the few pharmacological options for medical treatment of DYT1 dystonia,^{8,9} although their use is impeded by a number of serious adverse effects. The rationale behind the use of anticholinergic agents relies on the imbalance between striatal dopamine and acetylcholine (ACh), which results in an increased cholinergic tone.¹⁰⁻¹² Although cholinergic interneurons (ChIs) represent a minority of striatal neuronal population, they produce an extensive and dense innervation, providing the highest regional level of ACh and cholinergic markers in the brain and playing a central role in the integration of corticostriatal and thalamostriatal inputs with dopaminergic nigrostriatal innervation.^{13,14} In normal conditions, striatal cholinergic tone is downregulated either by acetylcholinesterases (AChE), ACh-degrading enzymes, or by the activation of both muscarinic M2/M4 autoreceptors (M2/M4 mAChR) and dopamine 2 receptors (D2R). Indeed, D2R activation normally reduces the frequency of spontaneous firing of ChIs and inhibits the release of ACh.¹⁵⁻¹⁷ There is now robust evidence for a fundamental alteration of D2R signaling in the DYT1 mouse striatum consisting in an excitation, rather than inhibition, of the firing frequency of striatal ChIs.^{18,19} The loss of the mutual control between striatal dopamine and ACh and the subsequent neurochemical imbalance are responsible for the impairment of bidirectional corticostriatal synaptic plasticity. Indeed, multiple DYT1 dystonia rodent models showed significant abnormalities in corticostriatal long-term synaptic plasticity, exhibiting the loss of both long-term depression (LTD) and synaptic depotentiation,²⁰⁻²⁴ as well as an enhanced long-term potentiation.^{20,21} Accordingly, these synaptic plasticity deficits could be compensated either by lowering ACh content or by antagonizing M1 muscarinic receptors.^{20,21,23,25}

Despite such extensive evidence, the nature of ACh dysregulation remains to be clarified. Here, we utilized a multidisciplinary approach to measure the possible changes in cholinergic markers, and their functional impact in the pathophysiology of dystonia, in the *Tor1a* null (*Tor1a*^{+/-}) mouse model.²⁶ These mice show a decrease in torsinA levels,¹⁹ as well as electrophysiological and molecular alterations common to multiple rodent models of DYT1 dystonia (for a review, see references 27-29). In *Tor1a*^{+/-}

mice, we identified a significant alteration in the expression of the striatal vesicular acetylcholine transporter (VAcHT), which loads ACh into the presynaptic vesicles before its release through exocytosis. Blockade of VAcHT restored long-term synaptic depression (LTD) alterations, indicating its functional relevance. Altogether, our results indicate that VAcHT is a potential target for pharmacological intervention.

Materials and Methods

Mouse Model

Male *Tor1a*^{+/-} null mice²⁶ (9- to 12-week-old, B6; 129-Tor1atm1Wtd/J, 006251 The Jackson Laboratory) and their wild-type littermates were used for the experiments. The experimental procedures were approved by the Institutional Ethical Review Committee and the Italian Ministry of Health (authorization no. 223/2017-PR) in accordance with the European Union and Italian directives (2010/63EU, D.Lgs 26/2014). The mouse strain was bred at Fondazione Santa Lucia Animal Facility. Mice were housed in groups of 4 per cage in a temperature-controlled room with 12-hour light-dark cycle. Water and food were provided ad libitum.

Electrophysiology

Mice were killed, and their brains were removed as previously described.³⁰ Corticostriatal coronal slices (220 μ m) were cut with a vibratome in oxygenated artificial cerebrospinal fluid (aCSF). Slices recovered for a minimum of 20 minutes and then were placed in a chamber superfused at 2.5 to 3.5 mL/min with oxygenated aCSF. ChIs were visualized with infrared-differential interference contrast (IR-DIC) videomicroscopy and identified based on both their large somatic size and their distinctive electrophysiological properties.³⁰⁻³² Electrophysiological signals were detected using Multiclamp 700B, AxoPatch 200, and Axoclamp B amplifiers (Molecular Devices, San Jose, CA, USA). For cell-attached patch-clamp recordings, electrodes (4–7 M Ω) were filled with a solution containing 125 mM K-gluconate, 1 mM CaCl₂, 2 mM MgCl₂, 0.1 mM 1,2-bis-o-aminophenoxy-ethane-N,N,N',N'-tetraacetic acid (BAPTA), 10 mM NaCl, 19 mM HEPES hemisodium salt (*N*-(2-hydroxyethyl)-piperazine-*N*-sulfonatesulfonic acid), 0.3 mM Na-guanosine triphosphate, and 2 mM Mg-adenosine triphosphate, pH 7.3. Inhibitory postsynaptic currents (IPSCs) were evoked in ChIs, during whole-cell patch-clamp recordings, by intrastriatal paired-pulse (50-ms interval) electrical stimulation in the presence of 6-cyano-7-nitroquinoxaline-2,3-dione (CNQX, 10 μ M) and D(-)-2-Amino-5-phosphopentanoic acid (D-AP5, 20 μ M) to avoid glutamate signaling contamination. Parasagittal striatal slices (290 μ m) were used for intracellular recordings, with sharp electrodes filled with 2 M KCl (50 M Ω). A bipolar

tungsten electrode was positioned in the *corpus callosum* white matter to activate corticostriatal fibers. Glutamatergic excitatory postsynaptic potentials (EPSPs) were evoked by 0.1-Hz electrical stimulation, in the presence of picrotoxin (50 μ M) in the perfusing solution, to block GABAA-mediated transmission.³⁰ High-frequency stimulation (HFS, three trains: 100 Hz, 3-second duration, 20-second interval) was delivered to induce LTD.

Confocal Imaging

Deeply anesthetized mice were perfused with 4% paraformaldehyde in 0.12 M sodium phosphate buffer (pH 7.5). Brains were postfixed overnight in the same solution and stored at 4°C. Thirty-micrometer sections were cut using a vibratome (SM 2010R, Leica, Milan, Italy) and maintained in 30% sucrose overnight at 4°C. Then sections were dehydrated with serial alcohol dilutions (50–70–50%) and incubated 1 hour at room temperature in a solution containing 10% donkey serum in phosphate-buffered saline (PBS) 0.25%-Triton X-100 (PBS-Tx). Finally, they were incubated 3 days at 4°C with the following primary antibodies: goat anti-ChAT (choline acetyltransferase) (1:500, NBPI30052, Novus Biologicals, Bio-Techne, Milan, Italy) and rabbit anti-VAcHT (1:500, 139103, Synaptic Systems, Goettingen, Germany). Sections were rinsed thrice for 10 minutes in Tris Buffered Saline (TBS) and incubated at room temperature for 2 hours with 1:200 Alexa 488 or Alexa 647 (Invitrogen, Thermo Fisher Scientific, Milan, Italy). Sections were rinsed for 10 minutes thrice in TBS before mounting with Super Frost Plus (Thermo Scientific, Rodano (MI) Italy). Images were acquired using an LSM700 Zeiss confocal laser scanning microscope (Zeiss, Milan, Italy); confocal images were acquired as previously described.^{31,33}

Immunoblotting

Dorsal striata were homogenized in lysis buffer (50 mM Tris-HCl pH 7.4, 150 mM NaCl, 1% Triton X-100, 0.25% Na deoxycholate, 5 mM MgCl₂, 0.1% sodium dodecyl sulfate, and 1 mM EDTA) supplemented with 1% protease inhibitor cocktail (Sigma-Aldrich, Merck, Milano, Italy). Lysates were sonicated, incubated 1 hour on ice, and then centrifuged at 14,000 rpm for 15 minutes at 4°C. Protein concentration was determined using the Bradford assay (Bio-Rad, Milan, Italy). NuPAGE LDS sample buffer (Invitrogen, Life Technologies), containing 100 mM 1,4-dithiothreitol (DTT), was added to the samples. Twenty-five micrograms of proteins were loaded onto sodium dodecyl sulfate polyacrylamide gel electrophoresis. Then, polyvinylidene fluoride membranes were probed with the following primary antibodies: anti-torsinA (1:800, ab34540, Abcam, Prodotti Gianni, Milan, Italy), anti-VGLUT3 (vesicular glutamate transporter 3) (1:000, 135203, Synaptic Systems, Goettingen, Germany), anti-CHT1 (62-2ES) (1:500,

SC33713, Santa Cruz, D.B.A., Milan, Italy), anti-ChAT (1:1000, NBP1-30052, Novus Biologicals, Bio-Techne, Milan, Italy), anti-VAcHT (1:1000, 139103, Synaptic Systems, Goettingen, Germany), and anti- β -actin (1:20,000, A5441, Sigma-Aldrich). Then, membranes were incubated for 1 hour at room temperature with secondary antibodies. The immunoblot bands were detected with a chemiluminescence system (iBright or film, Thermo Fisher Scientific, Milan, Italy), and their densities were quantified using ImageJ software, National Institutes of Health, USA. For pharmacological treatments with 10 μ M sulpiride or 10 μ M hemicholinium, 200- μ m thick dorsal striatum slices were incubated for 6 hours at 32°C in oxygenated aCSF and 1% protease inhibitor cocktail (Sigma-Aldrich). At the end of treatment, the tissue was immediately frozen in liquid nitrogen and stored at –80°C until sample preparation for immunoblotting.

Gene Expression Analysis by Real-Time Quantitative Polymerase Chain Reaction

Total RNA was extracted from dorsal striata using TRIreagent (Sigma-Aldrich, Merck, Milan, Italy) and quantified using an ND-1000 spectrophotometer (NanoDrop Technologies 2000C, Thermo Scientific, Milan, Italy). RNA integrity was confirmed by 2% agarose gel electrophoresis. Then, 1 mg of total RNA was treated with DNAase I (Invitrogen) and reverse transcribed to complementary cDNA (Roche Italia, Milan, Italy). Real-time PCR (polymerase chain reaction) was performed on 25 ng of cDNA using specific primers (assay ID 316836 Gene Symbol Slc18a3). Quantitative PCR reactions were carried out in duplicate using the SYBR Green I Master Mix (Roche) on a Roche Light Cycler LC480 system. The relative VAcHT gene expression was analyzed using the 2^(–ddCt) method.³⁴

Detection of ACh and AChE Activity

For AChE activity assay, mice were killed by cervical dislocation, their brains were removed, and dorsal striata were rapidly dissected at 0°C and stored at –80°C until further analysis. The AChE activity was determined by a colorimetric method, using the AChE assay kit (ab138871, Abcam). The striatal tissue was homogenized in lysis buffer supplemented with 1% protease inhibitor cocktail (Sigma-Aldrich), with a motor-driven pestle for three cycles, followed by alternate freezing and thawing of the samples. Dorsal striatum ACh levels were measured using a choline/ACh assay kit (ab65345, Abcam). Absorbance was measured using a Microplate Reader (Multiskan GO, Thermo Scientific). For the measurement of basal ACh content, slices (200–400 μ m thick) of dorsal striatum were immediately lysed; in another set of experiments, slices were incubated for 4 minutes at room temperature with 10 μ M quinpirole in oxygenated aCSF.

Drugs

Drugs were bath applied and diluted at the final concentration in aCSF. Vesamicol and neostigmine were obtained from Merck, Milan, Italy. Picrotoxin and donepezil were purchased from Bio-technie, Milan, Italy.

Statistical Analysis

Excitatory postsynaptic current (EPSC), Excitatory postsynaptic potential (EPSP), and action potential amplitudes were measured using Clampfit (pClamp 10, Molecular Devices). Statistical analysis was performed using GraphPad Prism. Data were obtained from at least three independent biological samples. All biological replicates are represented by “N,” number of animals, and “n,” number of cells. Values in the text and in the figures are presented as mean \pm standard error of the mean. Two-tailed paired or unpaired *t* test was used for two-sample comparisons. F test was used to compare dose–response curves. The significance level was set at $P < 0.05^*$, $P < 0.01^{**}$, and $P < 0.001^{***}$.

Results

VACHT Protein Level Is Increased in the Dorsal Striatum of Tor1a^{+/-} Mice

A functional cholinergic neurotransmission is maintained through an appropriate synthesis, vesicular packaging, and release of ACh. Our confocal microscope analysis showed that VACHT is localized to the soma of large-sized ChIs in Tor1a^{+/-} striatum, similar to wild-type mice (not shown) as well as to the known distribution of the ACh synthesizing enzyme ChAT (Fig. 1A–C). In addition, VACHT immunostaining was abundantly present in axonal varicosities, as punctiform labeling (Fig. 1B,C). Indeed, high-magnification images show coexpression of VACHT and ChAT in ChIs, consistent with previous observations.^{35,36}

We then evaluated CHT1, ChAT, and VACHT protein expression levels in the dorsal striatum. As previously reported, torsinA protein level was reduced in Tor1a^{+/-} mice compared to controls (Fig. 1D; $P < 0.0001^{***}$). CHT1 (Fig. 1E) and ChAT (Fig. 1F) protein levels were not significantly different in Tor1a^{+/+} versus Tor1a^{+/-} striatum (CHT1, $P = 0.47$; ChAT, $P = 0.85$). Striatal ChIs coexpress VGLUT3.^{37,38} VGLUT3 protein level was similar in the striatum of wild-type and mutant mice (Fig. 1G; VGLUT3, $P = 0.93$). VACHT immunoreactivity revealed an intense band at the predicted size of 70 kDa (Fig. 1H). Quantification of band intensity revealed a significant increase in VACHT protein level in Tor1a^{+/-} mice, as compared to Tor1a^{+/+} control mice (Fig. 1H; $P = 0.0176^*$). Therefore, we verified whether the

increase in VACHT protein abundance was caused by an enhancement in mRNA level. However, we found no difference in the expression of VACHT (*Slc18a3*) mRNA between Tor1a^{+/-} and Tor1a^{+/+} mice (Fig. 1I; $P = 0.23$). Our findings provide evidence for a selective increase in VACHT protein level in the dorsal striatum of Tor1a^{+/-} in spite of no significant changes in mRNA expression.

ACh Content Is Elevated in the Striatum of Tor1a^{+/-} Mice Both in Basal Condition and after D2R Activation

These findings prompted us to measure ACh content in striatal slices from Tor1a^{+/-} mice. To minimize ACh degradation, we quickly collected the samples in liquid nitrogen. By means of a colorimetric assay, we measured an increase in striatal ACh content in Tor1a^{+/-} with respect to wild-type mice (Fig. 2A; $P = 0.0293^*$). We previously found that the activation of D2R increases the frequency of ChI spontaneous firing activity in Tor1a^{+/-} mice,¹⁹ similar to that reported in multiple DYT1 models.^{12,18,21,32,39} To verify that D2R-dependent increase in firing frequency would result in an elevation in ACh release in Tor1a^{+/-} mice, we measured ACh content after striatal slice treatment with the D2R agonist quinpirole. Bath application of quinpirole (10 μ M, 4 minutes) did not significantly affect ACh content in wild-type slices, whereas it increased striatal ACh level in Tor1a^{+/-} striatum (Fig. 2B; $P = 0.001^{**}$). Overall, these data show that basal ACh content is enhanced in the striatum of Tor1a^{+/-} mice, in line with microdialysis experiments performed in Tor1a^{+/ Δ gag} mice.¹² Furthermore, our experiments demonstrate that D2R activation abnormally elevates ACh tone in Tor1a^{+/-} mice.

To investigate whether the abnormal D2R activity might cause the increase in VACHT protein level observed in Tor1a^{+/-} mice, we treated dorsal striatum slices with the D2R antagonist sulpiride (10 μ M, 6 hours, 32°C). This prolonged treatment did not alter VACHT protein level with respect to untreated, contralateral slices (Fig. S1A; Tor1a^{+/+} $P = 0.433$; Tor1a^{+/-} $P = 0.431$). There was no statistically significant difference in the effect of sulpiride on VACHT protein expression between genotypes ($P = 0.94$). To further rule out the role of the enhanced striatal ACh tone in the increase in VACHT, we performed a treatment of slices with hemicholinium (10 μ M, 6 hours, 32°C). Similar to sulpiride, hemicholinium did not alter VACHT protein level with respect to untreated, contralateral slices (Fig. S1B; Tor1a^{+/+} $P = 0.40$, Tor1a^{+/-} $P = 0.81$). There was no statistically significant difference in the effect of the treatment with hemicholinium between genotypes ($P = 0.63$).

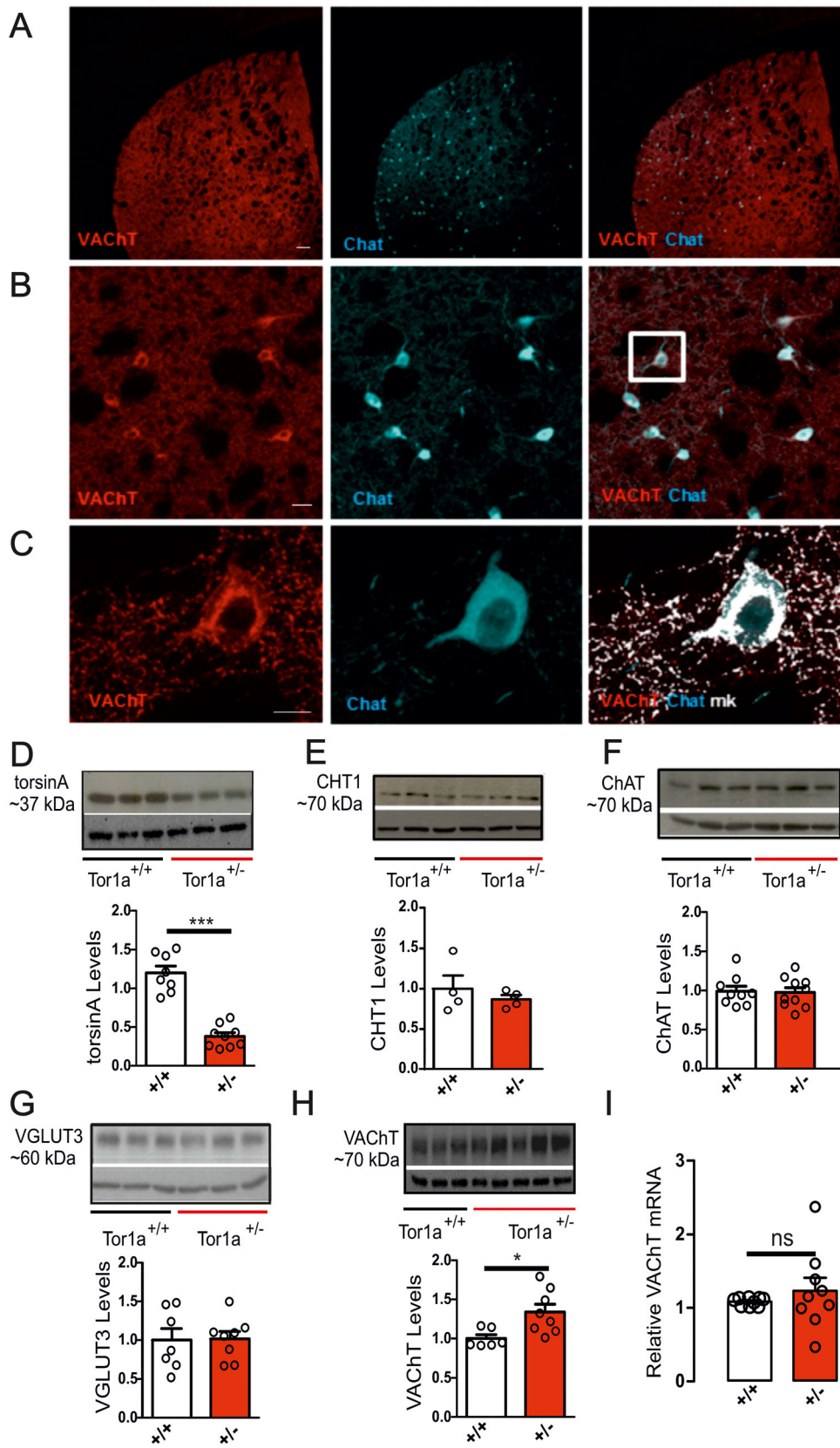


FIG. 1. Legend on next page.

AChE Activity Is Increased in *Tor1a*^{+/-} Mice

AChE is the enzyme that catalyzes the rapid breakdown of ACh in the striatum.^{40,41} By means of a colorimetric assay, we therefore measured the enzymatic

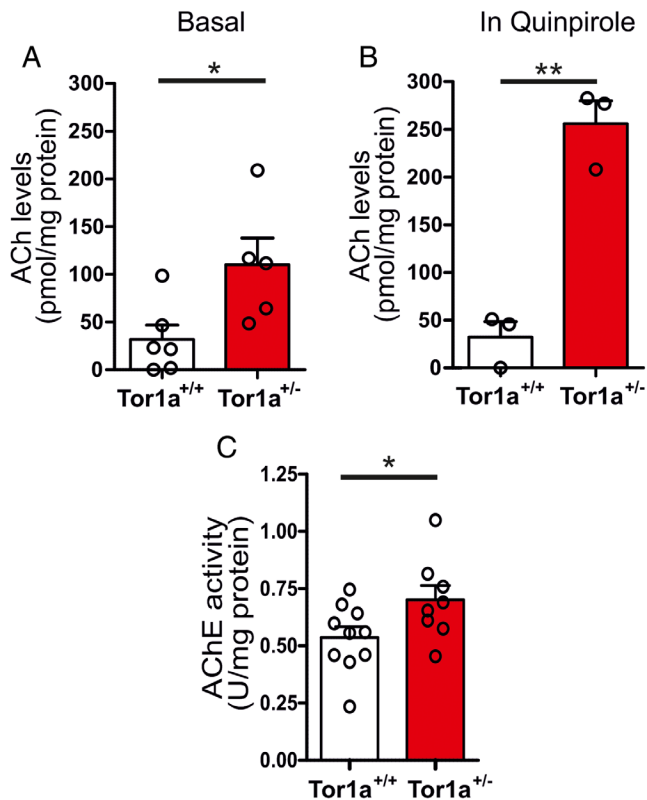


FIG. 2. Increased striatal ACh (acetylcholine) content and AChE (acetylcholinesterase) activity in *Tor1a*^{+/-} mice. VACHT (vesicular acetylcholine transporter) protein expression in vitro after ACh system modulation. **(A)** The histogram shows an enhanced basal ACh content in mutant mice (*Tor1a*^{+/-} 31.88 ± 15.01 pmol/mg protein, N = 6; *Tor1a*^{+/-} 110.1 ± 27.99 pmol/mg protein, N = 5; unpaired *t* test *P* = 0.0293). **(B)** Quinpirole (10 μM, 4 minutes) dramatically increases striatal ACh content in *Tor1a*^{+/-}, as compared to control, mice (*Tor1a*^{+/+} 32.34 ± 16.24 pmol/mg protein; N = 3; *Tor1a*^{+/-} 255.8 ± 24 pmol/mg protein in N = 3; unpaired *t* test *P* = 0.001*). **(C)** The plot shows a significant increase in AChE activity in the dorsal striatum of *Tor1a*^{+/-} mice (*Tor1a*^{+/+} 0.54 ± 0.05 U/mg total proteins, N = 10; *Tor1a*^{+/-} 0.70 ± 0.06 U/mg total proteins, N = 8; unpaired *t* test *P* = 0.048*). [Color figure can be viewed at wileyonlinelibrary.com]

activity and found a significant increase in AChE activity in *Tor1a*^{+/-} compared to wild-type mice (Fig. 2C; *P* = 0.048*). These results indicate that the increased rate of enzymatic degradation is likely a compensatory mechanism triggered by the elevation of basal ACh levels.

Reduced Potency of AChE Inhibitors on Spontaneous Firing Activity of *Tor1a*^{+/-} ChIs

ACh exerts an inhibitory feedback control on ChIs activity through the activation of M2/M4 mACh autoreceptors.⁴²⁻⁴⁴ To investigate whether the enhancement of striatal ACh content could be caused by an altered autoreceptor function, we carried out an electrophysiology analysis of ChI excitability, measuring the responses to autoreceptor agonists. All the recorded neurons exhibited typical morphological features, such as a large polygonal body and two to three dendritic branches, as well as characteristic electrophysiological properties. Basal spontaneous firing rates did not statistically differ between genotypes (*Tor1a*^{+/+} 2.76 ± 0.43 Hz, n = 34, N = 23; *Tor1a*^{+/-} 3.11 ± 0.40 Hz, n = 27, N = 25; unpaired *t* test, *P* = 0.56). Bath application of the M2/M4 mAChR agonist oxotremorine (Fig. 3A,B, OXO 600 nM, 2 minutes) induced a decrease in ChI spontaneous firing rate in both *Tor1a*^{+/+} and *Tor1a*^{+/-} mice (Fig. 3C; *P* = 0.51). A dose-response curve showed that OXO acts with the same efficacy in both genotypes (Fig. 3C; *P* = 0.51).

AChE inhibitors enhance striatal ACh level, which tonically activates mACh autoreceptors on ChIs. As expected, bath application of neostigmine (Neost, 10 nM, 5 minutes) produced a decrease in the number of spontaneous action potentials in *Tor1a*^{+/+} mice (Fig. 3D,F). Remarkably, Neost was less effective in reducing the average firing rate in *Tor1a*^{+/-} slices (Fig. 3E,F; *P* = 0.0034). Similarly, donepezil, a reversible AChE inhibitor, produced a transient decrease in the number of spontaneous action potentials in *Tor1a*^{+/+} mice (Fig. S2A,B; *P* = 0.0416*).

FIG. 1. VACHT (vesicular acetylcholine transporter) protein level is increased in the striatum of *Tor1a*^{+/-} mice. **(A)** Representative confocal fluorescence images of a corticostriatal coronal section confirming cell-specific expression of VACHT (red) in ChAT (choline acetyltransferase)-positive cells (cyan) (scale 5×, scale bar 200 μm). Note the absence of immunolabeling in the cortical area. **(B)** Higher-magnification images showing cholinergic interneurons located in the dorsal striatum (scale 20×, scale bar 50 μm). **(C)** Merged image of the two split channels (ChAT-cyan and VACHT-red) and the overlapping mask VACHT/ChAT (mk-white) to better visualize immunoreactivity of VACHT on ChAT-positive ChIs (cholinergic interneurons) (scale 63x21.5, scale bar 10 μm). **(D-H)** Representative Western blots (25 μg of total striatal extract) and the respective densitometry analysis. Histograms show the amount of protein relative to β-actin (42 kDa), used as an internal loading control, and normalized to the wild-type samples of the same experiment. **(D)** TorsinA (37 kDa) protein level was reduced in the dorsal striatum of *Tor1a*^{+/-} mice (*Tor1a*^{+/+} 1.20 ± 0.09, N = 8; *Tor1a*^{+/-} 0.38 ± 0.05, N = 9; unpaired *t* test *P* < 0.0001***). **(E)** CHT1 (~70 kDa), **(F)** ChAT (~70 kDa), and **(G)** VGLUT3 (vesicular glutamate transporter 3) (~60 kDa) quantification did not show significant changes in *Tor1a*^{+/-} striatum (CHT1, *Tor1a*^{+/+} 1.000 ± 0.163, N = 4; *Tor1a*^{+/-} 0.868 ± 0.053, N = 4, unpaired *t* test *P* = 0.47; ChAT, *Tor1a*^{+/+} 0.99 ± 0.06, N = 9; *Tor1a*^{+/-} 0.97 ± 0.06, N = 10; unpaired *t* test *P* = 0.85; VGLUT3, *Tor1a*^{+/+} 1.00 ± 0.15, N = 7; *Tor1a*^{+/-} 1.01 ± 0.10, N = 8; unpaired *t* test *P* = 0.93). **(H)** VACHT (~70 kDa) densitometry analysis revealed a significant increase in protein level in *Tor1a*^{+/-} mice (*Tor1a*^{+/+} 1.00 ± 0.05, N = 6; *Tor1a*^{+/-} 1.33 ± 0.10, N = 8; unpaired *t* test *P* = 0.0176*). Data are presented as mean ± standard error of the mean (SEM). **(I)** VACHT mRNA copy numbers in *Tor1a*^{+/-} and *Tor1a*^{+/+} striatal samples were determined by quantitative real-time polymerase chain reaction. The dot-plot graph shows the relative expression of VACHT mRNA normalized to the expression of the reference gene *Hprt1* for each sample. *Tor1a*^{+/-} values are presented as fold change (2^{-(ddCt)}) with respect to *Tor1a*^{+/+} samples. No statistically significant difference was found between genotypes (1.23 ± 0.18 fold change, N = 9, unpaired *t* test *P* = 0.23). Data are presented as mean ± SEM. [Color figure can be viewed at wileyonlinelibrary.com]

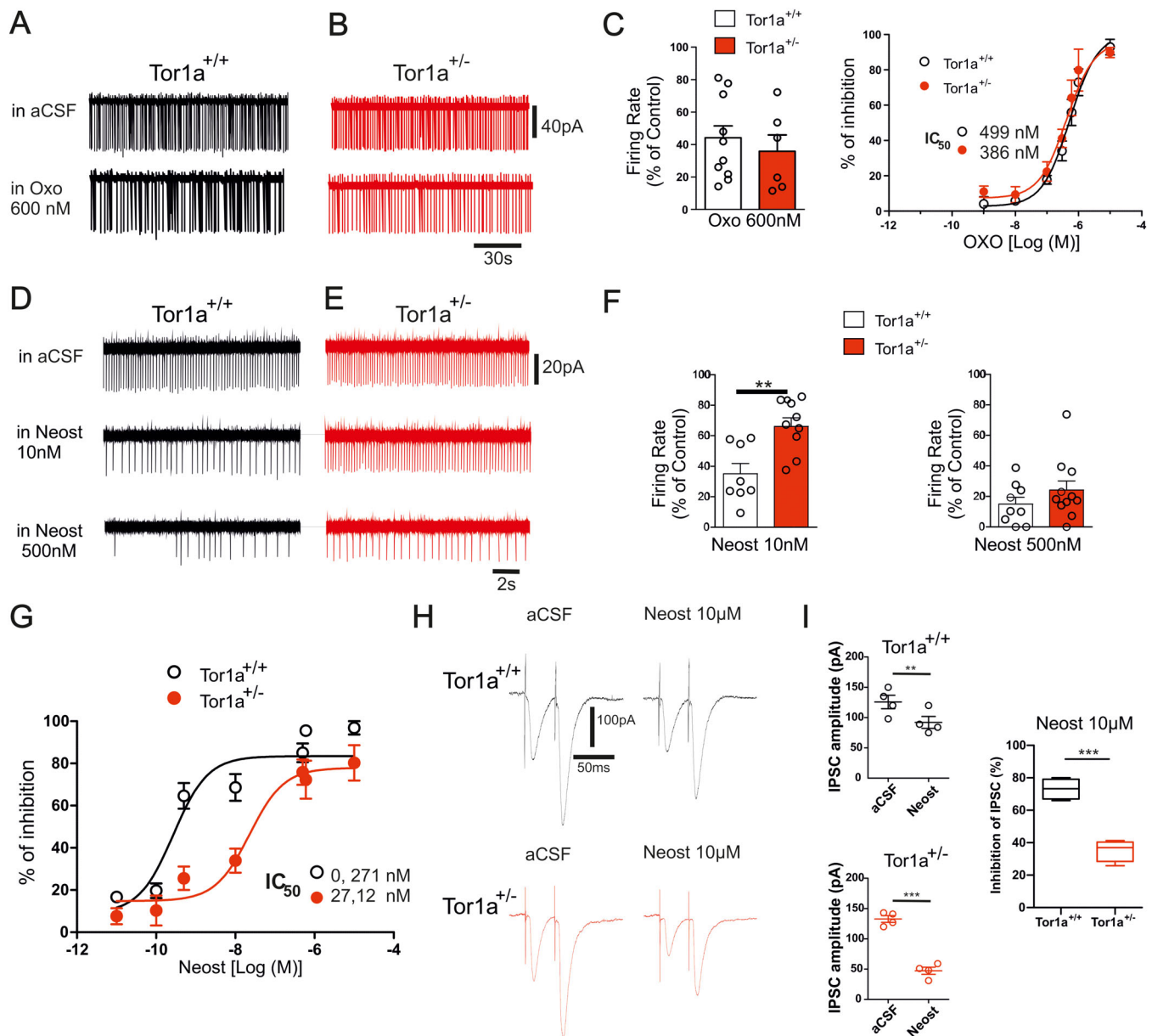


FIG. 3. Reduced potency of AChE (acetylcholinesterase) inhibitors on the spontaneous firing activity of $Tor1a^{+/-}$ Chls (cholinergic interneurons). **(A, B)** Representative patch-clamp recordings of Chls in aCSF (artificial cerebrospinal fluid) (top) and after bath application of oxotremorine (Oxo 600 nM, 2 minutes, bottom) in both strains. **(C)** (Left) Summary plot showing a similar decrease in firing rate induced by 600 nM Oxo in both genotypes ($Tor1a^{+/+}$: $44.15 \pm 7.35\%$ of control; $n = 11$, $N = 5$; $Tor1a^{+/-}$: $35.85 \pm 10.07\%$ of control; $n = 6$, $N = 3$; unpaired t test $P = 0.51$). (Right) The dose-response curves show similar kinetics of inhibition in both genotypes (IC_{50} : $Tor1a^{+/+}$ 499 nM, 95% confidence intervals: $3.463e-007$ to $7.212e-007$; $Tor1a^{+/-}$ 386 nM, $2.522e-007$ to $5.932e-007$; F test $P = 0.51$). **(D, E)** Representative traces of cell-attached recordings from Chls in aCSF (top) and after bath application of 10 nM (middle) and 500 nM (bottom) neostigmine (Neost, 5 minutes). **(F)** The histograms summarize the effect of 10 nM (left, $Tor1a^{+/+}$ $35.11 \pm 6.71\%$ of control, $n = 8$, $N = 6$; $Tor1a^{+/-}$ $66.07 \pm 5.69\%$ of control, $n = 9$, $N = 7$; unpaired t test $P = 0.0034^{**}$) and 500 nM of Neost (right, $Tor1a^{+/+}$ $14.98 \pm 4.44\%$ of control; $n = 9$, $N = 6$; $Tor1a^{+/-}$ $24.13 \pm 6.01\%$ of control; $n = 11$, $N = 8$; unpaired t test $P = 0.25$). **(G)** The dose-response curves of Neost inhibitory effect on Chl firing activity show a shift to the right in $Tor1a^{+/-}$ compared to wild-type cells ($Tor1a^{+/+}$: IC_{50} 0.271 nM, $1.119e-010$ to $6.598e-010$ confidence interval; $Tor1a^{+/-}$: IC_{50} 27.12 nM, $6.797e-009$ to $1.082e-007$ 95% confidence interval; F test $P < 0.0001^{***}$). **(H)** Representative traces of IPSCs (inhibitory postsynaptic currents) evoked in Chls by paired pulse intrastriatal stimulation (50-ms interval) in the presence of CNQX (10 μM) and D-AP5 (20 μM), to avoid glutamate signaling contamination, before (left) and after (right) bath application of Neost (10 μM, 15 minutes). **(I)** The graphs summarize the effect of Neost on the IPSC amplitude ($Tor1a^{+/+}$: in aCSF 125.8 ± 12 pA, in Neost 92 ± 10 pA, $n = 4$, paired t test $P = 0.0054^{**}$; $Tor1a^{+/-}$: in aCSF 132.8 ± 6 pA, in Neost 47.3 ± 6 pA, $n = 4$, paired t test $P = 0.019^{**}$). The extent of IPSC amplitude reduction is significantly higher in $Tor1a^{+/-}$ mice than in $Tor1a^{+/+}$ mice ($Tor1a^{+/+}$ $73.11 \pm 3.17\%$ of control, $n = 4$; $Tor1a^{+/-}$ $35.26 \pm 3.32\%$ of control, $n = 4$; unpaired t test $P = 0.0002^{***}$). Data are presented as mean \pm standard error of the mean. [Color figure can be viewed at wileyonlinelibrary.com]

Pretreatment with the nonselective mAChR antagonist scopolamine (3 μM, 20 minutes) abolished the inhibitory effect of neostigmine (10 nM, 5 minutes) (data not

shown). The inhibitory effect of a higher concentration of Neost on the firing rate (500 nM; Fig. 3D–F) was similar between genotypes (Fig. 3F; $P = 0.25$). As shown by the

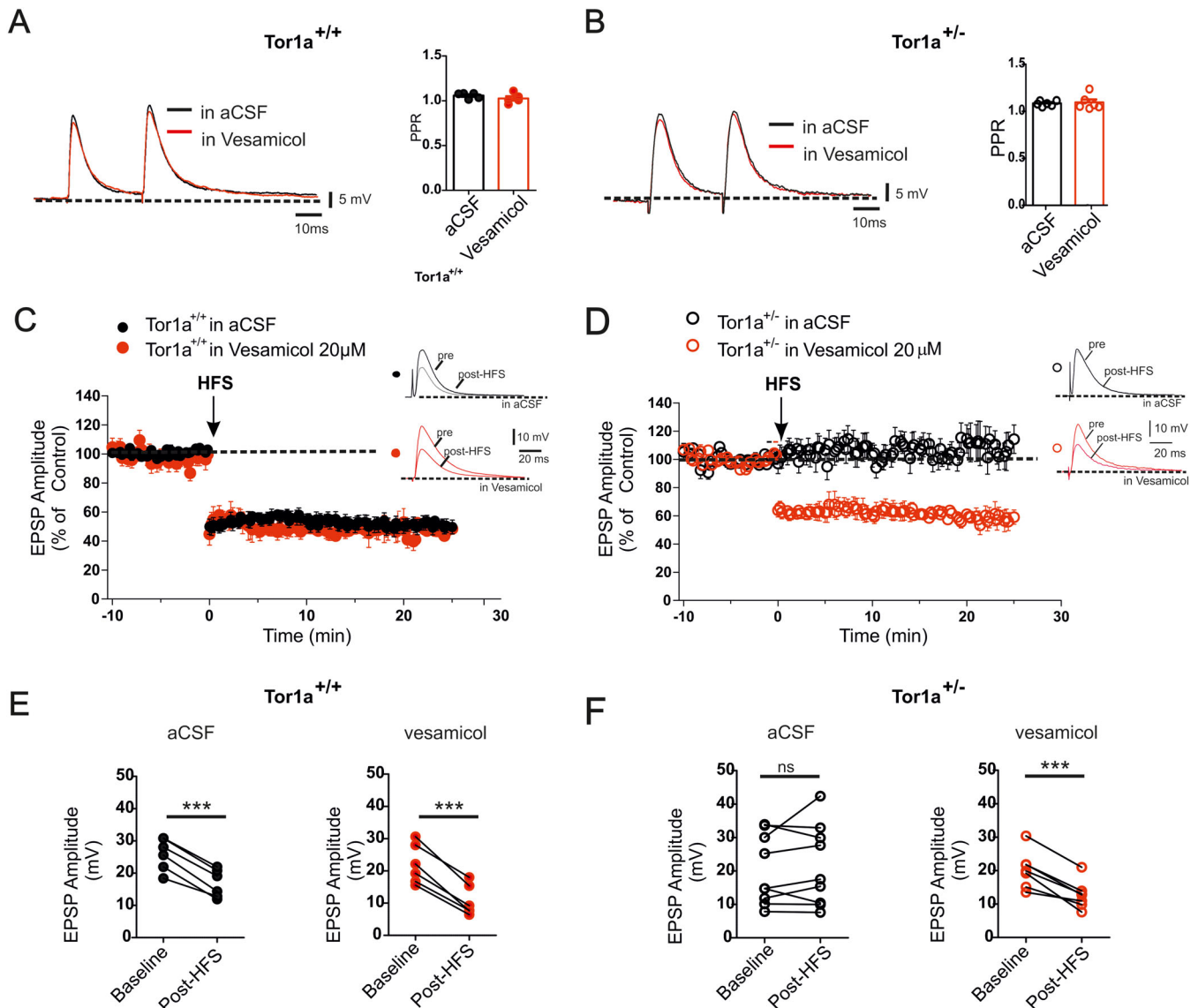


FIG. 4. Inhibition of VACHT (vesicular acetylcholine transporter) rescues LTD (long-term depression) in $Tor1a^{+/-}$ mice. **(A)** Slice perfusion with the VACHT-blocking agent vesamicol (20 μ M, 20 minutes) does not modify the paired-pulse ratio (PPR) of corticostriatal EPSPs (excitatory postsynaptic potentials) in $Tor1a^{+/+}$ MSNs, as shown by (left) the representative traces of intracellular recordings and (right) the summary plot (in aCSF [artificial cerebrospinal fluid] 1.06 ± 0.01 , $n = 5$, $N = 4$; in vesamicol 1.03 ± 0.03 , $n = 5$, $N = 4$; paired t test $P = 0.268$). **(B)** Vesamicol does not modify the PPR of corticostriatal EPSPs in $Tor1a^{+/-}$ MSNs: (left) representative traces of intracellular recordings and (right) summary plot (in aCSF 1.08 ± 0.01 , $n = 6$, $N = 4$; in vesamicol 1.09 ± 0.03 , $n = 6$, $N = 4$; paired t test $P = 0.682$). **(C)** Time course of corticostriatal LTD induced by HFS (high-frequency stimulation) (black arrow) in $Tor1a^{+/+}$ MSN, either in aCSF (black circles) or in 20- μ M vesamicol (red circles). **(D)** Time course of corticostriatal LTD, induced by HFS (black arrow) in $Tor1a^{+/-}$ MSN, either in aCSF (black circles) or in 20- μ M vesamicol (red circles). **(E)** The amplitude of $Tor1a^{+/+}$ corticostriatal LTD was similar in aCSF and in vesamicol (aCSF, black circles: pre-HFS 25.92 ± 2.04 mV; post-HFS 16.82 ± 1.76 mV; $n = 6$, $N = 4$; paired t test $P < 0.0001^{***}$; vesamicol, red circles: pre-HFS 22.05 ± 2.50 ; post-HFS 10.73 ± 1.95 mV; $n = 6$, $N = 5$; paired t test $P = 0.0002^{***}$). **(F)** HFS did not induce a corticostriatal LTD in $Tor1a^{+/-}$ MSNs (aCSF, black circles: pre-HFS 20.23 ± 3.48 mV; post-HFS 21.53 ± 4.04 mV; $n = 9$, $N = 5$; paired t test $P = 0.4555$). Vesamicol preincubation was able to rescue LTD expression in the striatum of $Tor1a^{+/-}$ mice (pre-HFS 20.25 ± 2.07 mV; post-HFS 12.74 ± 1.60 mV; $n = 7$, $N = 5$; paired t test $P = 0.0005^{***}$). [Color figure can be viewed at wileyonlinelibrary.com]

dose-response analysis (Fig. 3G), Neost-induced effects on firing rate were significantly different between $Tor1a^{+/-}$ and $Tor1a^{+/+}$ ChIs. The dose-response curve of $Tor1a^{+/-}$ mice was shifted to the right with an IC₅₀ value significantly higher with respect to $Tor1a^{+/+}$ (Fig. 3G; $P < 0.0001^{***}$), demonstrating that Neost acts with the same efficacy in both genotypes but with a lower potency in $Tor1a^{+/-}$.

Muscarinic M1 receptors were shown to modulate inhibitory inputs from GABAergic terminals targeting ChIs.⁴⁵ Thus, to further evaluate the effect of an abnormal ACh level on striatal circuitry, we investigated the modulatory role of ACh on the GABAergic transmission from striatal projection neurons and parvalbumin-expressing interneurons onto ChIs in both animal groups. IPSCs were evoked in ChIs by intra-striatal stimulation. In

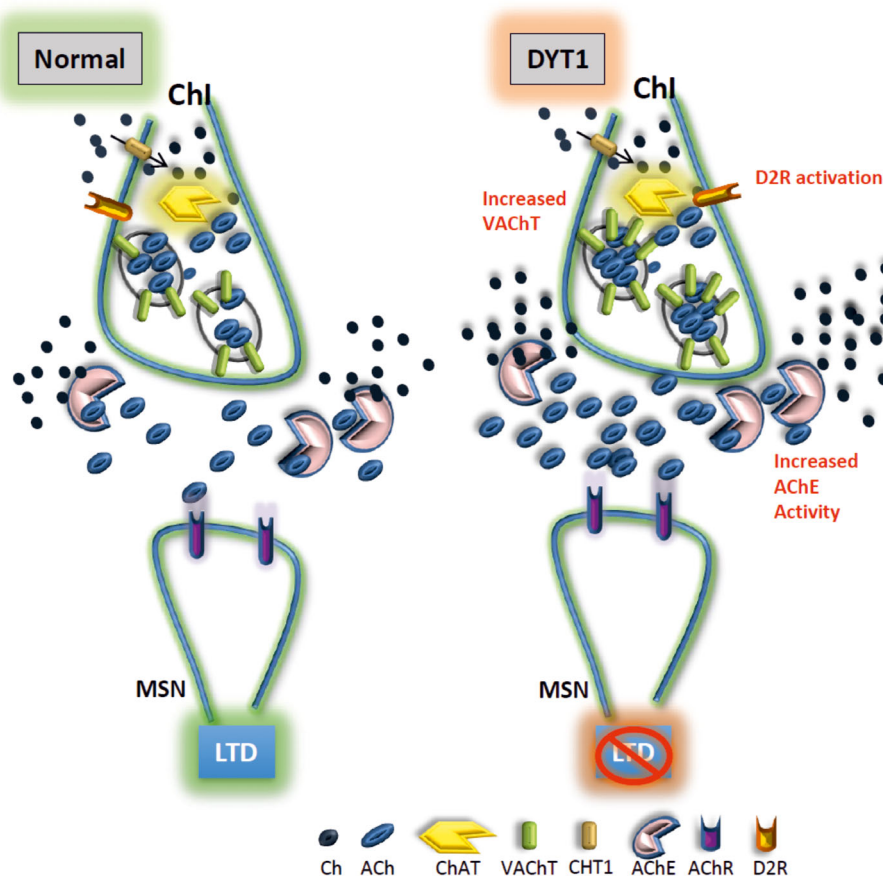


FIG. 5. Simplified model of cholinergic synaptic dysfunction in DYT1 dystonia. (Left) Cartoon showing normal signaling between ChIs (cholinergic interneurons) and MSNs, leading to the expression of normal LTD (long-term depression). In DYT1 dystonia (right), synaptic vesicles contain more VACHT (vesicular acetylcholine transporter), which allows to store significant amounts of ACh. During LTD induction, activation of an abnormal D2R (dopamine 2 receptor) increases the release of these vesicles fully loaded with ACh into the synaptic cleft. Despite the increase in AChE (acetylcholinesterase) activity, which helps degrading ACh, the excessive cholinergic tone disrupts the expression of synaptic plasticity in MSNs. [Color figure can be viewed at wileyonlinelibrary.com]

both $Tor1a^{+/+}$ and $Tor1a^{+/-}$ mice, the increase in intrastriatal ACh induced by bath application of neostigmine (10 μ M, 15 minutes) caused a significant decrease in IPSC amplitude (Fig. 3H; $Tor1a^{+/+}$ $P = 0.0054^{**}$; $Tor1a^{+/-}$ $P = 0.019^{**}$), which was significantly higher in $Tor1a^{+/-}$ than in $Tor1a^{+/+}$ mice (Fig. 3I; $P = 0.0002^{***}$), further supporting an increased ACh tone in DYT1 mice.

Altogether, our data indicate that mACh autoreceptor function is preserved in $Tor1a^{+/-}$ mice and suggest that AChE inhibition is less effective in modulating ChI firing activity because of the stable increase in enzymatic activity in $Tor1a^{+/-}$ mice.

Inhibition of VACHT Restores Striatal Long-Term Depression

A prominent involvement of cholinergic transmission in the impairment of striatal synaptic plasticity has been shown in DYT1 dystonia models, where a loss of corticostriatal LTD has been reported.^{20,21,23-25} We investigated whether, by blocking VACHT and therefore

reducing ACh uptake into synaptic vesicles and, in turn, ACh release, we might rescue corticostriatal LTD. EPSPs were evoked by 0.1-Hz stimulation of corticostriatal fibers. Slice perfusion with vesamicol (20 μ M, 20 minutes), a VACHT-blocking agent, did not modify the intrinsic membrane properties of medium spiny neurons (MSNs) (not shown), as well as the amplitude and paired-pulse ratio (PPR) of corticostriatal EPSPs in both genotypes (Fig. 4A,B; $Tor1a^{+/+}$ $P = 0.268$; $Tor1a^{+/-}$ $P = 0.682$).

As previously shown in multiple DYT1 rodent models,^{20-25,30} delivery of HFS induced an LTD in wild-type but not in $Tor1a^{+/-}$ MSNs (Fig. 4C,D, $Tor1a^{+/+}$ in aCSF: $P < 0.0001^{***}$; $Tor1a^{+/-}$ in aCSF: paired t test $P = 0.4555$). Of note, we found that 20- μ M vesamicol was able to rescue the expression of a robust synaptic depression in $Tor1a^{+/-}$ slices (Fig. 4D; $Tor1a^{+/-}$ in vesamicol: $P = 0.0005^{***}$), without affecting LTD in wild-type neurons (Fig. 4C; $Tor1a^{+/+}$ in vesamicol: $P = 0.0002^{***}$).

These data support the hypothesis that an increased presynaptic VACHT protein level elevates the vesicular

packaging of ACh, thus allowing an enhanced release in the dorsal striatum and generating an increased ACh tone, which prevents LTD induction (Fig. 5).

Discussion

The paucity of novel drugs for the treatment of dystonia is determined by the lack of definite therapeutic targets. Although dystonia is not typically associated with degeneration or obvious neuropathological features, striatal dysfunction, including abnormal cholinergic transmission, is consistently implicated in multiple forms of dystonia, including DYT1 dystonia. The aim of the present study was to better define the mechanistic basis for such abnormality in the DYT1 striatum. Our results indicate that the striatal cholinergic machinery is altered at multiple levels in *Tor1a^{+/-}* mice, ultimately producing a major elevation in ACh content.

ACh is synthesized by ChAT from the substrates choline (taken up into the cell by the high-affinity choline transporter CHT1) and acetylCoA. ACh is then packaged into vesicles by VACHT, which is encoded by a small gene embedded in the gene-producing ChAT, and its action is terminated by AChE. Although we found no significant differences in ChAT or CHT1 protein expression, we measured an increase in VACHT protein amounts in mutant mice, without changes in mRNA levels. In fact, protein abundance is regulated at different levels, including protein degradation.⁴⁶ The finding of an increased level of the transporter despite the fact that the synthesizing enzyme is unaffected is not surprising. Previous studies found that an increased protein level of VACHT does not imply the involvement of other cholinergic markers.^{36,47,48}

Given the critical role of VACHT in cholinergic signaling, as a rate-limiting factor for replenishing cholinergic vesicles, our data show that an increased VACHT activity may be able to sustain enhanced ACh storage and release from synaptic vesicles in *Tor1a^{+/-}* mice. These findings are in agreement with previous observations showing that a similar increase in VACHT protein level leads to an increase in cholinergic tone.^{48,49} Accordingly, transgenic VACHT-deficient mice show decreased basal and evoked ACh release in the striatum.⁵⁰ Furthermore, VACHT overexpression induces changes in the morphology of striatal ChIs.³⁶ Interestingly, these observations are consistent with a previous work reporting an enlargement of striatal ChIs in a knock-in mouse model of DYT1 dystonia.⁵¹

Spontaneous firing activity of ChIs ensures a basal cholinergic tone in the striatum,⁵²⁻⁵⁴ which is negatively modulated by M2/M4 muscarinic autoreceptors and D2R dopamine receptors. Basal firing frequency was not altered in *Tor1a^{+/-}* ChIs, and the muscarinic autoreceptor response was conserved, as previously

reported.^{12,19,55} AChE inhibition, by increasing endogenous ACh content, caused a decrease in ChI spontaneous firing activity in both wild-type and mutant striatal slices. However, the decrease in firing rate in *Tor1a^{+/-}* ChIs was less pronounced compared to *Tor1a^{+/+}*. This observation is in accordance with present data showing an increased AChE activity in *Tor1a^{+/-}* striatum and in line with previous reports from a different DYT1 mouse model.²⁰ We hypothesize that the lack of changes in ChIs basal firing frequency, despite an increased ACh tone, might be due to the overactivity of AChE, preventing an increased activation of muscarinic autoreceptors. Such an increase in AChE activity may represent a compensatory mechanism to limit the abundance of ACh in the synaptic cleft. The physiological relevance of the increased ACh tone was demonstrated by our observation that, on AChE maximal inhibition, the amplitude of GABAergic synaptic currents was decreased more in *Tor1a^{+/-}* than in wild-type ChIs.

Similar to M2/M4 autoreceptors, in physiological conditions also D2R activation exerts an inhibitory action on striatal ChI firing activity. However, in several DYT1 rodent models we and others reported that the activation of D2R causes a significant increase in ChI firing rate.^{12,18,19} Here we demonstrate that the activation of striatal D2R produces a significant increase in ACh content in striatal slices of *Tor1a^{+/-}* mice. Indeed, a “paradoxical excitation” of ChIs induced by the activation of D2R has been reported also in DYT6 and DYT25 mouse models of genetic dystonia.⁵⁶

In the striatum, dopaminergic and cholinergic signaling act synergistically and reciprocally to shape synaptic plasticity. In the *Tor1a^{+/-}* mouse model, we previously reported the loss of LTD and suggested that this impairment could result from a cholinergic overactivity, because it can be reverted by lowering ACh content or inhibiting postsynaptic muscarinic M1 receptors.²⁰ In support of this hypothesis, the present data show that VACHT inhibition by vesamicol was able to rescue LTD expression in *Tor1a^{+/-}* MSNs. Indeed, an increased level of VACHT protein allows either synaptic vesicles to be filled with more ACh or more vesicles to be filled and released, therefore supporting a sustained release under HFS. Because vesamicol did not change corticostriatal PPR, we hypothesize that VACHT inhibition, by limiting ACh release, may dampen the activation of postsynaptic M1 receptors located on MSNs, thus rescuing LTD expression, in accordance with our previous work.²⁵ Indeed, though the anticholinergic drug trihexyphenidyl, currently used in the management of dystonia, does not display selectivity for M1 receptors,⁵⁷ we showed that only M1-selective and M1-preferring antagonists were able to offset synaptic plasticity deficits in DYT1 mice.²⁵

The mechanisms by which mutant torsinA leads to the specific modification of cholinergic transmission with an increased protein level of VACHT and long-

lasting alterations in circuit function are still unknown. The high expression of torsinA in striatal ChIs might explain a preferential vulnerability of these neurons.^{11,58} Recent studies suggested a relationship between the loss of ChIs and the expression of a dystonia phenotype in torsinA conditional knockout models.^{59,60} However, there is little evidence supporting the degeneration of cholinergic neurons in DYT1 dystonia patients.⁵⁹ Histological studies in DYT1 patients' striata indicate a preservation of large aspiny interneurons, which are believed to correspond to ChIs.⁶¹⁻⁶³

Novel, selective VACHT Positron emission tomography (PET) ligands have been recently developed to measure cholinergic function in a number of conditions, including Parkinson's and Alzheimer's diseases.^{64,65} VACHT represents a promising target to measure cholinergic deficits in dystonia patients.^{66,67}

Overall, our findings provide a direct demonstration of a significant alteration of the cholinergic transmission in the striatum of DYT1 mice, further adding to substantial evidence in support of the central role of ACh in DYT1 dystonia pathophysiology. ■

Acknowledgments: We thank Mr. Massimo Tolu for his brilliant technical assistance and Dr. Cristina Riviello and Dr. Annarita Wirz for their excellent assistance with animal caring. We wish to thank Dr. Venturina Stagni for helpful discussion. Open Access Funding provided by Università degli Studi di Pavia within the CRUI-CARE Agreement. [Correction added on 19 May 2022, after first online publication: CRUI funding statement has been added

Data availability statement

Data available on request from the authors.

References

- Fahn S, Eldridge R. Definition of dystonia and classification of the dystonic states. *Adv Neurol* 1976;14:1-5.
- Ozelius LJ, Hewett JW, Page CE, et al. The early-onset torsion dystonia gene (DYT1) encodes an ATP-binding protein. *Nat Genet* 1997;17(1):40-48.
- Granata A, Koo SJ, Haucke V, et al. CSN complex controls the stability of selected synaptic proteins via a torsinA-dependent process. *EMBO J* 2011;30(1):181-193.
- Grillet M, Dominguez Gonzalez B, Sicart A, et al. Torsins are essential regulators of cellular lipid metabolism. *Dev Cell* 2016;38(3):235-247.
- Rose AE, Brown RSH, Schlieker C. Torsins: not your typical AAA+ ATPases. *Crit Rev Biochem Mol Biol* 2015;50(6):532-549.
- Laudermilch E, Schlieker C. Torsin ATPases: structural insights and functional perspectives. *Curr Opin Cell Biol* 2016;40:1-7.
- Gonzalez-Alegre P. Advances in molecular and cell biology of dystonia: focus on torsinA. *Neurobiol Dis* 2019;127:233-241.
- Jankovic J. Treatment of dystonia. *Lancet Neurol* 2006;5(10):864-872.
- Downs AM, Roman KM, Campbell SA, et al. The neurobiological basis for novel experimental therapeutics in dystonia. *Neurobiol Dis* 2019;130:104526.
- Pisani A, Bernardi G, Ding J, et al. Re-emergence of striatal cholinergic interneurons in movement disorders. *Trends Neurosci* 2007;30(10):545-553.
- Eskow Jaunarajs KL, Bonsi P, Chesselet MF, et al. Striatal cholinergic dysfunction as a unifying theme in the pathophysiology of dystonia. *Prog Neurobiol* 2015;127-128:91-107.
- Scarduzio M, Zimmerman CN, Jaunarajs KL, et al. Strength of cholinergic tone dictates the polarity of dopamine D2 receptor modulation of striatal cholinergic interneuron excitability in DYT1 dystonia. *Exp Neurol* 2017;295:162-175.
- Ding JB, Guzman JN, Peterson JD, et al. Thalamic gating of corticostriatal signaling by cholinergic interneurons. *Neuron* 2010;67(2):294-307.
- Sciamanna G, Tassone A, Mandolesi G, et al. Cholinergic dysfunction alters synaptic integration between thalamostriatal and corticostriatal inputs in DYT1 dystonia. *J Neurosci* 2012;32(35):11991-12004.
- Clos MV, García-Sanz A, Vivas NM, et al. D2 dopamine receptors and modulation of spontaneous acetylcholine (ACh) release from rat striatal synaptosomes. *Br J Pharmacol* 1997;122(2):286-290.
- DeBoer P, Heeringa MJ, Abercrombie ED. Spontaneous release of acetylcholine in striatum is preferentially regulated by inhibitory dopamine D2 receptors. *Eur J Pharmacol* 1996;317(2-3):257-262.
- Maurice N, Mercer J, Chan CS, et al. D2 dopamine receptor-mediated modulation of voltage-dependent Na⁺ channels reduces autonomous activity in striatal cholinergic interneurons. *J Neurosci* 2004;24(46):10289-10301.
- Pisani A, Martella G, Tschertner A, et al. Altered responses to dopaminergic D2 receptor activation and N-type calcium currents in striatal cholinergic interneurons in a mouse model of DYT1 dystonia. *Neurobiol Dis* 2006;24(2):318-325.
- Bonsi P, Ponterio G, Vanni V, et al. RGS9-2 rescues dopamine D2 receptor levels and signaling in DYT1 dystonia mouse models. *EMBO Mol Med* 2019;11(1):e9283.
- Martella G, Tassone A, Sciamanna G, et al. Impairment of bidirectional synaptic plasticity in the striatum of a mouse model of DYT1 dystonia: role of endogenous acetylcholine. *Brain* 2009;132(Pt 9):2336-2349.
- Martella G, Maltese M, Nisticò R, et al. Regional specificity of synaptic plasticity deficits in a knock-in mouse model of DYT1 dystonia. *Neurobiol Dis* 2014;65:124-132.
- Grundmann K, Glöckle N, Martella G, et al. Generation of a novel rodent model for DYT1 dystonia. *Neurobiol Dis* 2012;47(1):61-74.
- Dang MT, Yokoi F, Cheetham CC, et al. An anticholinergic reverses motor control and corticostriatal LTD deficits in Dyt1 ΔGAG knock-in mice. *Behav Brain Res* 2012;226(2):465-472.
- Rittiner JE, Caffall ZF, Hernández-Martinez R, et al. Functional genomic analyses of Mendelian and sporadic disease identify impaired eIF2α signaling as a generalizable mechanism for dystonia. *Neuron* 2016;92(6):1238-1251.
- Maltese M, Martella G, Madeo G, et al. Anticholinergic drugs rescue synaptic plasticity in DYT1 dystonia: role of M1 muscarinic receptors. *Mov Disord* 2014;29(13):1655-1665.
- Goodchild RE, Kim CE, Dauer WT. Loss of the dystonia-associated protein torsinA selectively disrupts the neuronal nuclear envelope. *Neuron* 2005;48(6):923-932.
- Imbriani P, Ponterio G, Tassone A, et al. Models of dystonia: an update. *J Neurosci Methods* 2020;339:108728.
- Tassone A, Sciamanna G, Bonsi P, et al. Experimental models of dystonia. *Int Rev Neurobiol* 2011;98:551-572.
- Meringolo M, Tassone A, Imbriani P, et al. Dystonia: are animal models relevant in therapeutics? *Rev Neurol* 2018;174(9):608-614.
- Maltese M, Stanic J, Tassone A, et al. Early structural and functional plasticity alterations in a susceptibility period of DYT1 dystonia mouse striatum. *Elife* 2018;7:e33331.
- Ponterio G, Tassone A, Sciamanna G, et al. Enhanced mu opioid receptor-dependent opioidergic modulation of striatal cholinergic transmission in DYT1 dystonia. *Mov Disord* 2018;33(2):310-320.
- Sciamanna G, Hollis R, Ball C, et al. Cholinergic dysregulation produced by selective inactivation of the dystonia-associated protein torsinA. *Neurobiol Dis* 2012;47(3):416-427.

33. Vanni V, Puglisi F, Bonsi P, et al. Cerebellar synaptogenesis is compromised in mouse models of DYT1 dystonia. *Exp Neurol* 2015; 271:457–467.
34. Livak KJ, Schmittgen TD. Analysis of relative gene expression data using real-time quantitative PCR and the 2(-Delta Delta C(T)) method. *Methods* 2001;25(4):402–408.
35. Gangarossa G, Guzman M, Prado VF, et al. Role of the atypical vesicular glutamate transporter VGLUT3 in l-DOPA-induced dyskinesia. *Neurobiol Dis* 2016;87:69–79.
36. Janickova H, Prado VF, Prado MAM, et al. Vesicular acetylcholine transporter (VACHT) over-expression induces major modifications of striatal cholinergic interneuron morphology and function. *J Neurochem* 2017;142(6):857–875.
37. Gras C, Amillon B, Lepicard EM, et al. The vesicular glutamate transporter VGLUT3 synergizes striatal acetylcholine tone. *Nat Neurosci* 2008;11(3):292–300.
38. El Mestikawy S, Wallén-Mackenzie A, Fortin GM, et al. From glutamate co-release to vesicular synergy: vesicular glutamate transporters. *Nat Rev Neurosci* 2011;12(4):204–216.
39. Sciamanna G, Tassone A, Martella G, et al. Developmental profile of the aberrant dopamine D2 receptor response in striatal cholinergic interneurons in DYT1 dystonia. *PLoS One* 2011;6(9):e24261.
40. Hebb CO, Silver A. Gradient of choline acetylase activity. *Nature* 1961;189:123–125.
41. Macintosh FC. The distribution of acetylcholine in the peripheral and the central nervous system. *J Physiol (London)* 1941;99(4):436–442.
42. Bonsi P, Martella G, Cuomo D, et al. Loss of muscarinic autoreceptor function impairs long-term depression but not long-term potentiation in the striatum. *J Neurosci* 2008;28(24):6258–6263.
43. Goldberg JA, Ding JB, Surmeier DJ. Muscarinic modulation of striatal function and circuitry. *Handb Exp Pharmacol* 2012;208:223–241.
44. Mamaligas AA, Ford CP. Spontaneous synaptic activation of muscarinic receptors by striatal cholinergic neuron firing. *Neuron* 2016;91(3):574–586.
45. Suzuki E, Momiyama T. M1 muscarinic acetylcholine receptor-mediated inhibition of GABA release from striatal medium spiny neurons onto cholinergic interneurons. *Eur J Neurosci* 2021;53(3): 796–813.
46. Vogel C, Marcotte EM. Insights into the regulation of protein abundance from proteomic and transcriptomic analyses. *Nat Rev Genet* 2012;13(4):227–232.
47. Guzman MS, De Jaeger X, Raulic S, et al. Elimination of the vesicular acetylcholine transporter in the striatum reveals regulation of behaviour by cholinergic-glutamatergic co-transmission. *PLoS Biol* 2011;9(11):e1001194.
48. Nagy PM, Aubert I. Overexpression of the vesicular acetylcholine transporter increased acetylcholine release in the hippocampus. *Neuroscience* 2012;218:1–11.
49. Prado VF, Roy A, Kolisnyk B, et al. Regulation of cholinergic activity by the vesicular acetylcholine transporter. *Biochem J* 2013;450(2):265–274.
50. Prado VF, Martins-Silva C, de Castro BM, et al. Mice deficient for the vesicular acetylcholine transporter are myasthenic and have deficits in object and social recognition. *Neuron* 2006;51(5): 601–612.
51. Song C-H, Bernhard D, Bolarinwa C, et al. Subtle microstructural changes of the striatum in a DYT1 knock-in mouse model of dystonia. *Neurobiol Dis* 2013;54:362–371.
52. Bolam JP, Wainer BH, Smith AD. Characterization of cholinergic neurons in the rat neostriatum. A combination of choline acetyltransferase immunocytochemistry, Golgi-impregnation and electron microscopy. *Neuroscience* 1984;12(3):711–718.
53. Wilson CJ, Chang HT, Kitai ST. Firing patterns and synaptic potentials of identified giant aspiny interneurons in the rat neostriatum. *J Neurosci* 1990;10(2):508–519.
54. Wilson CJ. The mechanism of intrinsic amplification of hyperpolarizations and spontaneous bursting in striatal cholinergic interneurons. *Neuron* 2005;45(4):575–585.
55. Liu Y, Xing H, Sheng W, et al. Alteration of the cholinergic system and motor deficits in cholinergic neuron-specific Dyt1 knockout mice. *Neurobiol Dis* 2021;2021:105342.
56. Eskow Jaunarajs KL, Scarduzio M, Ehrlich ME, et al. Diverse mechanisms lead to common dysfunction of striatal cholinergic interneurons in distinct genetic mouse models of dystonia. *J Neurosci* 2019; 39(36):7195–7205.
57. Dong GZ, Kameyama K, Rinken A, Haga T. Ligand binding properties of muscarinic acetylcholine receptor subtypes (m1-m5) expressed in baculovirus-infected insect cells. *J Pharmacol Exp Ther* 1995;274(1):378–384.
58. Augood SJ, Martin DM, Ozelius LJ, et al. Distribution of the mRNAs encoding torsinA and torsinB in the normal adult human brain. *Ann Neurol* 1999;46(5):761–769.
59. Pappas SS, Darr K, Holley SM, et al. Forebrain deletion of the dystonia protein torsinA causes dystonic-like movements and loss of striatal cholinergic neurons. *Elife* 2015;4:e08352.
60. Yokoi F, Oleas J, Xing H, et al. Decreased number of striatal cholinergic interneurons and motor deficits in dopamine receptor 2-expressing-cell-specific Dyt1 conditional knockout mice. *Neurobiol Dis* 2020;134:104638.
61. McNaught KSP, Kapustin A, Jackson T, et al. Brainstem pathology in DYT1 primary torsion dystonia. *Ann Neurol* 2004;56(4):540–547.
62. Pratt D, Mente K, Rahimpour S, et al. Diminishing evidence for torsinA-positive neuronal inclusions in DYT1 dystonia. *Acta Neuropathol Commun* 2016;4(1):85.
63. Sharma N. Neuropathology of dystonia. *Tremor Other Hyperkinet Mov (NY)* 2019;9:569.
64. Giboureau N, Som IM, Boucher-Arnold A, et al. PET radioligands for the vesicular acetylcholine transporter (VACHT). *Curr Top Med Chem* 2010;10(15):1569–1583.
65. Bohnen NI, Kanel P, Zhou Z, et al. Cholinergic system changes of falls and freezing of gait in Parkinson's disease. *Ann Neurol* 2019; 85(4):538–549.
66. Mazere J, Dilharreguy B, Catheline G, et al. Striatal and cerebellar vesicular acetylcholine transporter expression is disrupted in human DYT1 dystonia. *Brain* 2021;144(3):909–923.
67. Albin RL, Cross D, Cornblath WT, et al. Diminished striatal [123I] iodobenzovesamicol binding in idiopathic cervical dystonia. *Ann Neurol* 2003;53(4):528–532.

Supporting Data

Additional Supporting Information may be found in the online version of this article at the publisher's web-site.